A fuzzy approach to LPFG-based optical sensor processing and interrogation

Felipe Oliveira Barino, Eduardo Pestana de Aguiar, Leonardo de Mello Honório, Vinicius Nunes Henrique Silva, Andrés Pablo López-Barbero, Alexandre Bessa dos Santos

***Abstract*—In this work we report on a new interrogation method for Long-period fiber grating (LPFG) sensors. This type of sensor has been gaining increasing attention due its several interesting practical and metrological advantages. However, the LPFG optical signal is complex and could be difficult to process. We present a novel approach to the LPFG resonant wavelength detection and tracking using a multi-filter LPFG interrogator. Multi-filter LPFG interrogators present a great solution for LPFG sensor interrogation because there is no need for a priori knowledge concerning the LPFG sensor spectrum. We present a novel source-compensating preprocessing and a fuzzy inference system to track the LPFG resonant wavelength. Our proposal was compared to two baseline models: a simple linear regression and an artificial neural network. Our results showed the new approach could reduce resonant wavelength uncertainty by almost three times comparing to results found in the literature.**

***Index Terms*—optical fiber sensor, optical signal processing, optical spectrum measurement, long-period fiber grating, sensor readout, fiber Bragg gratings, fuzzy system**

I. INTRODUCTION

LONG-PERIOD fiber gratings (LPFGs) have been used as sensors for a wide variety of measurands. This type of sensor has been proposed in several contexts, from structural health monitoring [1]–[3] to chemical and bio sensing [4]–[6]. One could attribute the LPFG sensor's popularity to its intrinsic fiber-sensing advantages such as low noise, electromagnetic immunity, and high sensitivity. Moreover, LPFGs present some interesting advantages over other popular fiber grating sensors, like fiber Bragg gratings (FBGs), for example. These advantages are the intrinsic surrounding refractive index (SRI) sensitivity [7] and its complex transmission spectra. While the former allows for a wide range of applications, the latter could be used to perform multi-parameter sensing and self-compensation [8]–[13].

Beyond the applicability and metrological advantages, one could argue LPFGs are also easier to manufacture than FBGs. Note that both share roughly the same principle of operation, they are in-fiber diffraction gratings that promote mode coupling. But the FBG grating period (usually half a wavelength) is three orders of magnitude smaller than an LPFG grating period (typically hundreds of microns), therefore expensive equipment and complex techniques is often needed for FBG manufacturing. On the other hand, complex LPFG structures can be manufactured by simple point-by-point inscription methods using devices as simple as a fusion splicer [14].

The basic operation of an LPFG sensor relies on the energy coupling between the fundamental core mode of single-mode optical fiber to its evanescent cladding modes. This coupling occurs for specific wavelengths that satisfy the phase-matching condition:

$$\lambda_{res}^{m} = \left(n_{eff,co} - n_{eff,cl}^{m}\right)\Lambda \qquad (1)$$

where $n_{eff,co}$ and $n_{\mathrm{eff,cl}}$ are, respectively, the core and cladding effective index, Λ is the grating period, λ_{res} is the resonant wavelength and m denotes the coupling order.

The energy coupled to the cladding mode is abruptly attenuated due to scattering at the cladding/surrounding interface, thus attenuation bands centered at λ_{res}^{m} are seen in an LPFG transmission spectrum [15], [16].

From an instrumentation and measurement point of view, the resonant wavelength is the most important spectral characteristic of an LPFG. Indeed, the resonant wavelength changes with temperature, strain, and SRI [7]. Thus, it is used to calibrate the LPFG sensor to the desired measurand [17].

Therefore the resonant wavelength identification is crucial for LPFG sensor readout. This process is called interrogation and the instrument used to acquire the resonant wavelength is called interrogator. Several approaches have been proposed since the introduction of LPFG sensors, the trivial approach is to use an optical spectrum analyzer (OSA) to measure the LPFG transmission spectrum and retrieve the resonant wavelength by finding the attenuation dip's position. However, an OSA is bulky, expensive, and slow for a variety of in-field applications, thus researchers have found different

This work was supported in part by Inerge-UFJF, CNPq, CAPES, and Ambev.

Felipe Oliveira Barino is with Department of Circuits, Federal University of Juiz de Fora, Brazil (e-mail: felipe.barino@engenharia.ufjf.br).

Eduardo Pestana de Aguiar is with the Department of Industrial and Mechanical Engineering, Federal University of Juiz de Fora, Brazil

Leonardo de Mello Honório is with the Department of Energy, Federal University of Juiz de Fora, Brazil.

Vinicius Nunes Henrique Silva is with the Department of Telecommunications, Fluminense Federal University , Brazil

Andrés Pablo López-Barbero is with the Department of Telecommunications , Fluminense Federal University , Brazil

Alexandre Bessa dos Santos is with the Department of Circuits, Federal University of Juiz de Fora, Brazil

Color versions of one or more of the figures in this article are available online at http://ieeexplore.ieee.org

solutions to LPFG interrogation.

Instead of acquiring the whole LPFG attenuation dip, optical filters have been used to acquire the optical power at specific wavelengths and correlate its change to the resonant wavelength [18]–[20]. However, the filters positioning is heavily dependent on the LPFG transmission spectrum, thus the interrogator might be restricted to a single LPFG or a small resonant wavelength dynamic range after recalibration for a different sensor.

Therefore, filter-based interrogators are usually tailored to a single sensor and, although they tend to be cheaper, they lack generalization. To overcome this drawback, the use of a filter bank or even multiple sources has been proposed. These multi-filter LPFG interrogators use several optical power readings to estimate the LPFG spectrum by curve fitting, such as the reported in [21]. A similar approach is to use modulated optical sources to generate the multiple optical power readings to be passed to the curve fitting algorithm [22], [23]. Or using sparse filtering by means of several FBGs and machine learning to process the filtered data [24], [25].

In this work, we revisit the hardware presented in [25] and propose a novel processing scheme for the power read by the FBG array. The interrogator proposed in this work shares the same optics and electronics as the previously proposed. Nevertheless, it showed better precision and model interpretability while presenting the same generalization capability.

The novelty of this work is related to the FBG-array data preprocessing and resonant wavelength estimation. We propose a preprocessing step that minimizes the optical source dependency, normalizes the input data, and provides instinctively interpretable data. Concerning the resonant wavelength estimation, we present the use of a fuzzy inference system to output $\hat{\lambda}_{res}$ based on the preprocessed data. Therefore, we present a novel method for detection and tracking of an LPFG resonant wavelength, which implies on a novel readout method for sensors based on these devices.

II. Methods

A. The Data

We used the same dataset as [25]. The data was acquired by a multi-filter interrogator composed of 13 FBG modules. Each module contains an FBG centered at λ_{Bragg_i} $(i = 1, \dots, 13)$, coupled to an optical circulator and photodetector. The interrogator optical hardware is schematized in Fig. 1. Using this hardware, 528 pairs of input-output were collected, where the input is the 13 power readings from the optical setup and the output is the actual LPFG resonant wavelength. From the 528 pairs, there was data from 83 different LPFGs under different circumstances.

The dataset was randomly split into a train set and a test set, containing 369 (~70%) and 159 (~30%) pairs, respectively. All the analysis presented in this paper was made using the train set. The test set was only used to estimate the performance of models, to reduce bias when designing the models.

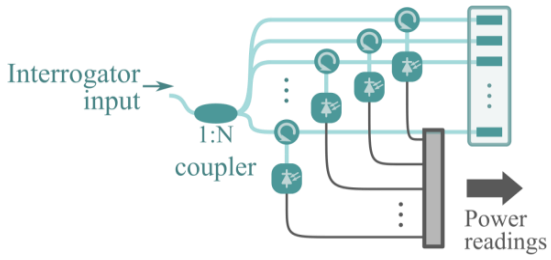

Fig. 1. Schematic of the interrogator hardware.

B. FBG-array data preprocessing

While in [25] the data was simply normalized before it was used as input to the multilayer perceptron, in this work we propose a different and more robust preprocessing. First let us assume, with no loss of generality, that the optical source used to illuminate the LPFG sensor is known and that the interrogator was used to acquire its power readings. This is a reasonable assumption because acquiring the power readings for the source could be performed by simply connecting it directly to the interrogator.

Let $\boldsymbol{x}_{LPFG}$ and $\boldsymbol{x}_{source}$ be the interrogator power readings for an LPFG sensor and the optical source, respectively. The preprocessing first step is to reduce the source interference on the power readings, thus obtaining $\boldsymbol{x}_s = \boldsymbol{x}_{source} - \boldsymbol{x}_{LPFG}$. Note that instead of subtracting the source from the LPFG, we subtracted the LPFG from the source. Therefore, where we should see a dip in $\boldsymbol{x}_{LPFG}$, we should see a peak in $\boldsymbol{x}_s$. Finally, we scale $\boldsymbol{x}_s$ by its sum. Hence, the full preprocessing of $\boldsymbol{x}_{LPFG}$ is given by:

$$\boldsymbol{x} = \frac{x_{source} - x_{LPFG}}{\sum_{i=1}^{13} x_{i_{source}} - x_{i_{LPFG}}} \quad (2)$$

The preprocessing of an example spectrum can be seen in Fig. 2. Before the preprocessing, $\boldsymbol{x}_{LPFG}$ represents the optical power of the LPFG spectrum at the position of each FBG filter. After the procedure, we get $\boldsymbol{x}$, which represents how close the LPFG resonant wavelength is to each FBG filter. For example, if $x_i = 1$, λ_{res} would be positioned coincidently with

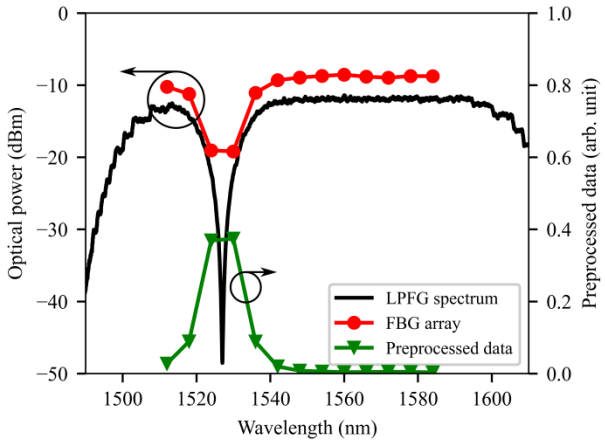

Fig. 2. Data preprocessing.

λ_{Bragg_i}. Similarly, if $x_i = x_{i+1} = 0.5$, λ_{res} would be positioned at the mean between λ_{Bragg_i} and $\lambda_{Bragg_{i+1}}$.Therefore, $\boldsymbol{x}$ provides a meaningful information about the LPFG position, and more easily interpretable than the raw $\boldsymbol{x}_{LPFG}$ data. Moreover, the effects related to optical source power fluctuations are minimized

Note that these examples are unlikely to happen, given the relationship between the typical LPFG FWHM and the FBG filters spacing. But practical values should appear as a superposition of these two examples. Note in Fig. 2 that $x_3 \approx x_4 < 0.5$ but $x_2 \approx x_5$, with λ_{res} roughly between λ_{Bragg_3} and λ_{Bragg_4}. Therefore, for the other case, if $\lambda_{res} \approx \lambda_{Bragg_i}$, we should see a high value for x_i and a smaller $x_{i-1} \approx x_{i+1}$.

For instance, this transformation should allow for easier resonant wavelength detection. With knowledge of the FBGs position, given by the vector containing each Bragg wavelength, namely $\boldsymbol{\lambda}_{FBG}$,. One should be able to perform a reasonable estimation of the LPFG resonant wavelength by the dot product $\boldsymbol{x} \cdot \boldsymbol{\lambda}_{FBG}$. Indeed, this weighted mean uses the fundamental principle of $\boldsymbol{x}$, i.e., how close the LPFG resonant wavelength is to each FBG filter. Later in this paper, we will discuss this relationship, as it is the foundation of the linear regression baseline model.

A summary of the preprocessed train set can be seen in Fig. 3. In this figure, one can see the relationship between the preprocessed value for each input (i.e. FBG position) and the LPFG resonant wavelength.

C. *The fuzzy inference system*

Fuzzy sets, logic and systems have a wide variety of uses. Some of their advantages are the robustness of the fuzzy sets, easy integration of multiple inputs, interpretability of the system, easy transfer learning from an expert to the system, and easy maintenance. Some applications within the instrumentation and measurement field are failure analysis [26], energy management in wireless sensor networks [27], soft-sensing [28], [29], and sensor fusion [30], [31], for example.

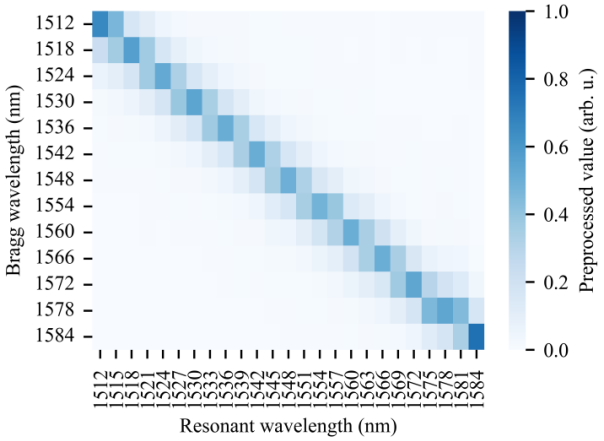

Fig. 3. Mean preprocessed values showing the relationship between the interrogator's input ($\boldsymbol{y}$-axis) and desired output ($\boldsymbol{x}$-axis).

In this work, we propose the use of a multi-input single-output (MISO) fuzzy inference system (FIS), using a Mamdani inference engine [32], to perform LPFG sensor readout. Fuzzy logic has already been used in optical sensing to estimate impact localization using FBGs [33], to monitor mechanical fingers using FBGs [34], to reconstruct dynamic deformations [35], and to process LPFG data and estimate axial stress [36].

Fig. 4 shows the proposed FIS for the interrogator. The input, i.e., the preprocessed data, is fuzzified; then the fuzzy variables are passed to the inference engine, activating the output fuzzy sets accordingly to the rule base; finally, the output sets are defuzzified to output the resonant wavelength crisp value.

We used three fuzzy sets to describe each input variable. All fuzzy sets were described by a double-variance modified gaussian membership function. Unlike the traditional gaussian membership function, we used a variance σ_1^2 for values below the mean μ, and another variance σ_2^2 for values above the mean; thus, the input membership functions might be asymmetric.

The input fuzzy sets were: FAR (F), NEAR (N), and CENTERED (C). These linguistic variables represent whether the LPFG resonant wavelength is far from the input filter (F), near the filter (N), or centered at the filter (C). Based on the analysis of Fig. 3, we saw the input value x_i is generally greater than 0.5 when $\lambda_{res} \approx \lambda_{Bragg_i}$, whereas the other inputs had values below 0.2. We also noted $x_i \approx x_{i+1}$ bigger than 0.3 when λ_{res} was between λ_{Bragg_i} and $\lambda_{Bragg_{i+1}}$. Given this knowledge, we were able to determine the membership functions shown in Fig. 5a.

The output sets were named $\Lambda_i, i = 0, \ldots, 24$. They were represented by 25 trapezoidal membership functions, which can be seen in Fig. 5b. These output membership functions were centered from 1512 to 1584 nm with 3 nm spacing, the same values shown at the Fig. 3 x-axis. The top and base of each trapezium were 1.25 nm 5.00 nm wide, respectively. We used the weighted average method to perform the defuzzification of the activated output fuzzy sets.

Concerning the rules, we were able to identify two main groups of situations: (i) when the resonant wavelength overlaps an input filter and (ii) when the resonant wavelength is between two input filters. We already discussed these situations in Section 2.2, and practical measurements should

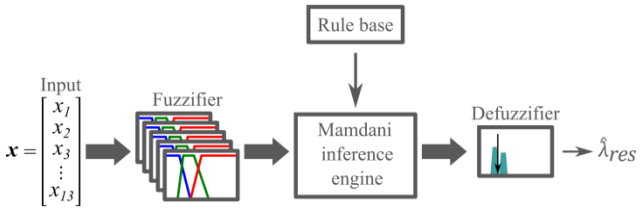

Fig. 4. Block diagram of the proposed fuzzy inference system.

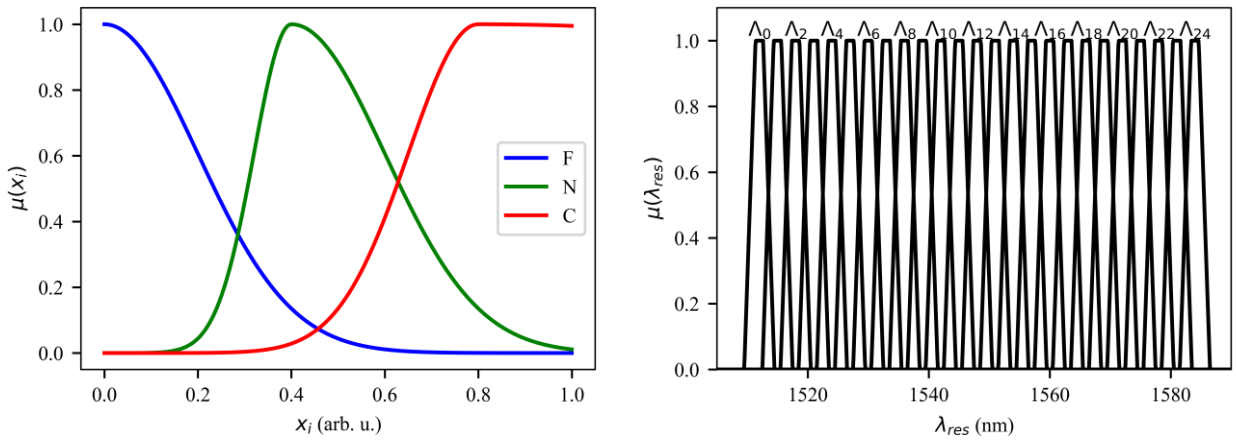

(a) (b)

Fig. 5. Membership functions of the (a) input fuzzy sets and (b) output fuzzy sets.

be a superposition of such groups.

Therefore, we created two groups of rules, to cover situations (i) and (ii). So, the rule base used in our FIS is given by group (i) rules:

IF $(x_i \text{ is } C)$ and $\left(x_j \text{ is } F, \forall j \neq i\right)$ THEN $(\lambda_{res} \text{ is } \Lambda_{2i})$ $\forall\, i \in 0, 1, \dots, 12$

and group (ii) rules:

IF $(x_i \text{ is } N)$ and $(x_{i+1} \text{ is } N)$ THEN $(\lambda_{res} \text{ is } \Lambda_{2i+1})$ $\forall\, i \in 0, 1, \dots, 11$

The Mamdani inference system used the min and max operators for t-norm and t-conorm, respectively. In addition to the membership functions shown in Fig. 5, we also tested a system with input membership functions optimized by genetic algorithm (GA) [37]. Some parameters of the set FAR were kept fixed, namely $\sigma_1 = \mu = 0$. The search interval for the others was $\sigma_1, \sigma_2 \in [0, 0.5]$ and $\mu \in [0.2, 0.8]$ for NEAR, whereas for CENTERED the search space was $\sigma_1 \in [0.1,1]$, $\sigma_2 \in [0.1,3]$, and $\mu \in [0.5, 1]$.

The optimization algorithm was configured as follows: a total of 200 individuals was randomly initiated and optimized for 100 epochs. The parameters were coded into a numerical vector. The mutation frequency was 0.05 and half of the population was substituted to their 100 most fitted children at the end of each epoch. The crossover function was the random weighted mean:

$$x_{child} = \frac{a x_{parent_1} + b x_{parent_2}}{a+b} \qquad (3)$$

with a, b randomly chosen in $(0,1]$.

The fitness function was the mean squared error (MSE) of the resonant wavelength estimated by the fuzzy system using the population-based input membership functions at the fuzzification step. A stopping criterion was created to stop the optimization when an MSE improvement of less than 0,0001 nm² was obtained between the most fitted individual of two consecutive epochs.

Therefore, two fuzzy inference systems were designed and tested in this work: the FIS expert gaussian and the FIS optimized gaussian; the former used the gaussian membership functions shown in Fig. 5a, whereas the latter used the GA-optimized gaussian membership functions. A comparison between these two sets of membership functions is presented at the beginning of the results section.

D. Baseline models

The proposed fuzzy models were compared to two baseline models and to results found in the literature. We propose a simple, yet efficient, baseline model based on the proposed preprocessing paradigm. Note that, the preprocessed data is normalized by the sum of the filtered power, therefore the sum of all inputs post-preprocessing is one. Therefore, it represents the percentual contribution of each FBG in the λ_{res} estimation.

Hence, we propose a linear model based on the dot product between the preprocessed data and the FBGs position vector, thus resulting in a weighted sum. To improve the model, and reduce bias, we performed a linear regression to this weighted sum, so the linear model is given by:

$$\hat{\lambda}_{res_{linear}} = a\left(\boldsymbol{x} \cdot \boldsymbol{\lambda_{Bragg}}\right) + b \qquad (4)$$

where a and b were calculated by the least square method using the train data and $\boldsymbol{\lambda_{Bragg}}$ is the vector of the interrogator's FBGs positions.

We also compare the proposed FIS models to the multi-layer perceptron (MLP) proposed in [25]. To make the comparison fair, we also retrained the MLP using data preprocessed by the new preprocessing method proposed in this work. The MLP is a $13 \times 5 \times 1$ network using the rectified linear unit activation function and it was trained using the same procedure and parameters used in the previous work.

E. Model evaluation

To evaluate and compare the proposed models to the baseline models we considered the following evaluation metrics: mean absoluter error (MAE) and mean squared error (MSE) to evaluate the models, as well as the mean (μ) and standard deviation (σ) of residuals.

To better characterize the interrogator error and its resilience to input noise we added white gaussian noise (AWGN) to the FBG filtered power. Moreover, to further

investigate how the models are impacted by noise, we tested the interrogator under several signal-to-noise ratio (SNR).

III. Results

In this section, we show the results obtained in our experiments and compare the proposed fuzzy approach to the baseline models and to the results found in the literature. First, let us analyze the results of the input membership function optimization. Therefore, we shall compare the input membership functions of the two proposed FIS systems.

Fig. 6 shows the expert-defined input membership functions in dotted lines and the GA-optimized in solid lines. We could see a considerable difference between the membership functions of the sets F and C. We also saw an increase in the N membership function asymmetry, with a bigger σ_2 while μ remained similar to the value defined by the expert analysis of the data shown in Fig. 3.

This difference suggests the mean values shown in Fig. 3 tended to underestimate the F behavior and overestimate the C behavior, whereas the N membership was underestimated for bigger input values.

Applying the two FISs, the linear model and the retrained MLP to the test data we obtained the evaluation metrics shown in Table I. Comparing the results reported in [25] with the most simple baseline model proposed in this work, using the new preprocessing step, we already saw a great improvement on the evaluation metrics. Note that the MAE, MSE, and uncertainty are greatly reduced using the novel preprocessing step and the proposed linear model when compared to the MLP used in [25]. This reduction implies the proposed preprocessing step improves the relationship between the FBG array data and the LPFG resonant wavelength.

Now we compare the proposed FIS models, the FIS expert gaussian and the FIS opt. gaussian, with the baseline models that use the same preprocessing step. Note that the distribution of the residuals is more spread out for the linear, MLP, FIS expert, and FIS optimized, in that order, as the MSE and σ shown in Table I suggested.

A comparison between the target λ_{res} and the residuals can be seen in Fig. 7. The estimated resonant wavelength was obtained by ten measurements under noise (SNR=10 dB). These results show great agreement between the real LPFG resonant wavelength and the estimated one, for all models. Indeed, the models' mean behavior is close to zero. We also estimated an $R^2 > 0.996$ for all models, so they explain well the LPFG resonant wavelength. Note that some models present more variance along with its mean behavior, i.e., the points are more spread out; indeed, see the σ and MSE found in Table I.

TABLE I
Proposed Models Evaluation Metrics

	Ref. [25]	Linear model	MLP	FIS expert	FIS GA opt.
MAE (nm)	1.00	0.762	0.668	0.443	0.352
MSE (nm^2)	1.98	0.979	0.737	0.317	0.242
μ (nm)	-0.033	-0.031	-0.083	-0.124	-0.101
σ (nm)	1.41	0.989	0.854	0.549	0.481

Finally, we analyze the relationship between the MSE and SNR. We calculated the test set MSE under each SNR, this experiment was repeated 100 times for each SNR (with resampled AWGN) and the estimated MSE can be seen in Fig. 8. One can see the FIS models are less sensitive to input noise.

The results found in this work showed the proposed novel preprocessing method provided easy to interpret and process information for the LPFG resonant wavelength. The performance improvement, compared to the work found in [25], using the simple linear model with this novel preprocessing method supported this assumption.

We also found the proposed fuzzy inference system outperformed the other baseline models, including the retrained MLP, which had the same structure proposed in [25]. The FIS with optimized membership functions showed nearly two times (1.8) better uncertainty than the MLP. Therefore, indicating a superior performance for the proposed fuzzy

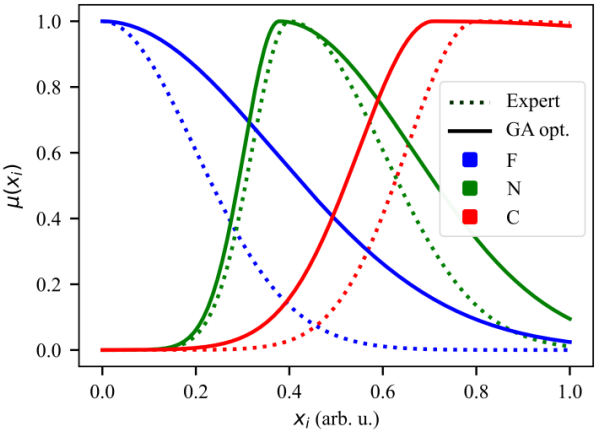

Fig. 6. Comparison between the expert defined and G.A. optimized input membership functions.

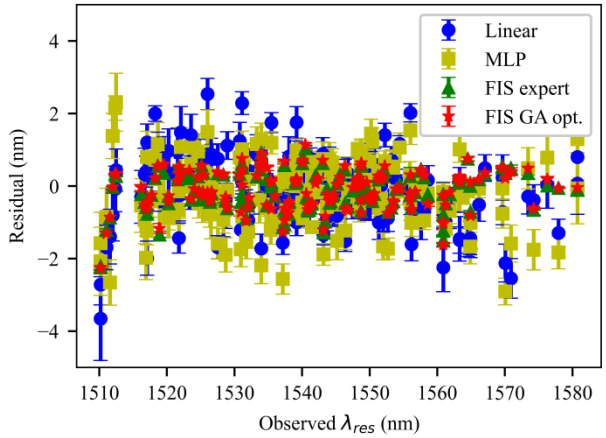

Fig. 7. Relationship between the observed and residual resonant wavelength.

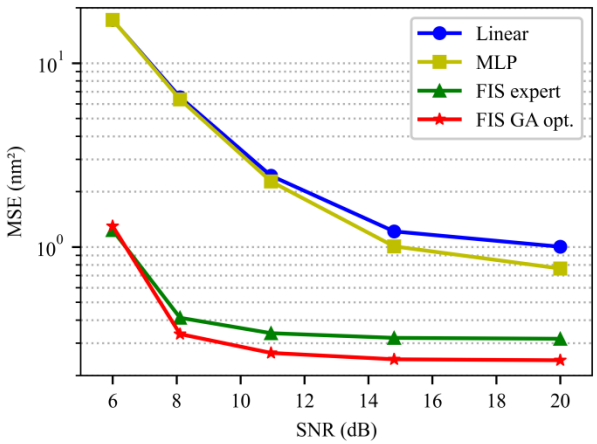

Fig. 8. Relationship between MSE and SNR.

approach to the problem.

IV. Conclusion

In this work, we presented the LPFG interrogation problem. We focused on the multi-filter approach to this problem and proposed two improvements to a previously reported LPFG interrogator: a better preprocessing of the filtered data and a novel processing model based on fuzzy inference.

We showed and discussed the preprocessing method, its foundations and the meaning of the preprocessed data. Moreover, we provided a visualization of this preprocessed data. We also presented the fuzzy inference system design, the in and out fuzzy sets, its membership function, and the rule base. Concerning the FIS, we also disused about the input membership functions optimization using genetic algorithms.

Furthermore, the results obtained using our novel proposals were compared to several models. We found the preprocessing method provides easier to process data, with a simple linear (baseline) model using this novel method outperforming a previously reported neural network. Our results also showed the FIS is a suitable and preferable candidate to process the multi-filter interrogator data, especially under noisy inputs. The results showed great improvement at the interrogator uncertainty when using the FIS approach and excellent resilience to noise. Moreover, fuzzy systems are easy to interpret, maintain, adjust, and even without any optimization could outperform the neural network used as baseline model in this work. The positives results found in this work also support the benefits of this interrogation approach, since the improvements observed were obtained by application of more robust processing methods, therefore proving the interrogator to have great scalability.

References

[1] S. Zheng, “Long-period fiber grating moisture sensor with nano-structured coatings for structural health monitoring,” *Struct. Heal. Monit. An Int. J.*, vol. 14, no. 2, pp. 148–157, Mar. 2015, doi: 10.1177/1475921714560069.

[2] Y. Huang, F. Tang, X. Liang, G. Chen, H. Xiao, and F. Azarmi, “Steel bar corrosion monitoring with long-period fiber grating sensors coated with nano iron/silica particles and polyurethane,” *Struct. Heal. Monit. An Int. J.*, vol. 14, no. 2, pp. 178–189, Mar. 2015, doi: 10.1177/1475921714560070.

[3] F. O. Barino *et al.*, “Loading Condition Estimation Using Long-Period Fiber Grating Array,” *IEEE Sens. J.*, vol. 21, no. 5, pp. 6202–6208, Mar. 2021, doi: 10.1109/JSEN.2020.3042779.

[4] B. Xu, J. Huang, L. Ding, H. Zhang, and H. Zhang, “A Sensitive Ammonia Sensor Using Long Period Fiber Grating Coated With Graphene Oxide/Cellulose Acetate,” *IEEE Sens. J.*, vol. 21, no. 15, pp. 16691–16700, Aug. 2021, doi: 10.1109/JSEN.2021.3081745.

[5] M. Janczuk-Richter *et al.*, “Long-period fiber grating sensor for detection of viruses,” *Sensors Actuators B Chem.*, vol. 250, pp. 32–38, Oct. 2017, doi: 10.1016/j.snb.2017.04.148.

[6] F. Esposito *et al.*, “Real time and label-free detection of C-reactive protein in serum by long period grating in double cladding fiber,” in *Optical Sensors 2021*, Apr. 2021, p. 23, doi: 10.1117/12.2589969.

[7] Xuewen Shu *et al.*, “Sensitivity characteristics of long-period fiber gratings,” *J. Light. Technol.*, vol. 20, no. 2, pp. 255–266, 2002, doi: 10.1109/50.983240.

[8] J. Hromadka *et al.*, “Multi-parameter measurements using optical fibre long period gratings for indoor air quality monitoring,” *Sensors Actuators B Chem.*, vol. 244, pp. 217–225, 2017.

[9] F. S. Delgado and A. B. dos Santos, “Multi-measurement scheme for a fiber-optic sensor based on a single long-period grating,” *J. Mod. Opt.*, vol. 64, no. 21, pp. 2428–2432, Nov. 2017, doi: 10.1080/09500340.2017.1367854.

[10] F. O. Barino, G. Ébias, J. Bittencourt, D. Discini, and A. B. Santos, “Two-dimensional long-period fiber grating sensor for touch applications,” *Microw. Opt. Technol. Lett.*, vol. 63, no. 2, pp. 647–652, Feb. 2021, doi: 10.1002/mop.32599.

[11] M. N. Ng, Z. Chen, and K. S. Chiang, “Temperature compensation of long-period fiber grating for refractive-index sensing with bending effect,” *IEEE Photonics Technol. Lett.*, 2002, doi: 10.1109/68.986813.

[12] C. Trono, F. Baldini, M. Brenci, F. Chiavaioli, and M. Mugnaini, “Flow cell for strain- and temperature-compensated refractive index measurements by means of cascaded optical fibre long period and Bragg gratings,” *Meas. Sci. Technol.*, 2011, doi: 10.1088/0957-0233/22/7/075204.

[13] Y.-P. Wang, L. Xiao, D. N. Wang, and W. Jin, “Highly sensitive long-period fiber-grating strain sensor with low temperature sensitivity,” *Opt. Lett.*, 2006, doi: 10.1364/ol.31.003414.

[14] C. Du, Q. Wang, S. Hu, and Y. Zhao, “Simultaneous measurement of refractive index and temperature based on a long period fiber grating inscribed in a photonic crystal fiber with an electric-arc discharge,” *Instrum. Sci. Technol.*, vol. 47, no. 2, pp. 185–194,

Mar. 2019, doi: 10.1080/10739149.2018.1508033.

[15] V. Bhatia and A. M. Vengsarkar, "Optical fiber long-period grating sensors," *Opt. Lett.*, vol. 21, no. 9, p. 692, May 1996, doi: 10.1364/OL.21.000692.

[16] T. Erdogan, "Fiber grating spectra," *J. Light. Technol.*, vol. 15, no. 8, pp. 1277–1294, 1997.

[17] G. R. C. Possetti, R. C. Kamikawachi, M. Muller, and J. L. Fabris, "Metrological Evaluation of Optical Fiber Grating-Based Sensors: An Approach Towards the Standardization," *J. Light. Technol.*, vol. 30, no. 8, pp. 1042–1052, Apr. 2012, doi: 10.1109/JLT.2011.2167500.

[18] H. J. Patrick, G. M. Williams, A. D. Kersey, J. R. Pedrazzani, and A. M. Vengsarkar, "Hybrid fiber Bragg grating/long period fiber grating sensor for strain/temperature discrimination," *IEEE Photonics Technol. Lett.*, vol. 8, no. 9, pp. 1223–1225, Sep. 1996, doi: 10.1109/68.531843.

[19] T. Allsop, T. Earthrowl, R. Reeves, D. J. Webb, and I. Bennion, "The interrogation and multiplexing of long period grating curvature sensors using a Bragg grating based, derivative spectroscopy technique," *Meas. Sci. Technol.*, vol. 15, no. 1, p. 44, 2003.

[20] J. P. Carvalho *et al.*, "Long-Period Gratings Dynamic Interrogation With Modulated Fiber Bragg Gratings and Optical Amplification," *IEEE Sens. J.*, vol. 12, no. 1, pp. 179–183, Jan. 2012, doi: 10.1109/JSEN.2011.2128305.

[21] H. Guo, G. Xiao, and J. Yao, "Interrogation of a Long Period Grating Fiber Sensor With an Arrayed-Waveguide-Grating-Based Demultiplexer Through Curve Fitting," *IEEE Sens. J.*, vol. 8, no. 11, pp. 1771–1775, Nov. 2008, doi: 10.1109/JSEN.2008.2004472.

[22] P. S. S. dos Santos, P. A. S. Jorge, J. de Almeida, and L. Coelho, "Low-Cost Interrogation System for Long-Period Fiber Gratings Applied to Remote Sensing," *Sensors*, vol. 19, no. 7, p. 1500, Mar. 2019, doi: 10.3390/s19071500.

[23] L. H. Silva, P. Santos, L. C. C. Coelho, P. Jorge, and J. M. Baptista, "Development of a Long Period Fiber Grating Interrogation System Using a Multimode Laser Diode," *Sensors*, vol. 21, no. 3, p. 749, Jan. 2021, doi: 10.3390/s21030749.

[24] M. A. Jucá, D. B. Haddad, A. B. Santos, and A. B. dos Santos, "Interrogation system for optical sensor using filter bank and artificial neural network," *Microw. Opt. Technol. Lett.*, vol. 62, no. 12, pp. 4015–4020, Dec. 2020, doi: 10.1002/mop.32516.

[25] F. O. Barino, A. B. d. Santos, and A. B. dos Santos, "LPG Interrogator Based on FBG Array and Artificial Neural Network," *IEEE Sens. J.*, vol. 20, no. 23, pp. 14187–14194, Dec. 2020, doi: 10.1109/JSEN.2020.3007957.

[26] A. Geramian, A. Shahin, B. Minaei, and J. Antony, "Enhanced FMEA: An integrative approach of fuzzy logic-based FMEA and collective process capability analysis," *J. Oper. Res. Soc.*, vol. 71, no. 5, pp. 800–812, May 2020, doi: 10.1080/01605682.2019.1606986.

[27] P. Nayak and B. Vathasavai, "Energy Efficient Clustering Algorithm for Multi-Hop Wireless Sensor Network Using Type-2 Fuzzy Logic," *IEEE Sens. J.*, vol. 17, no. 14, pp. 4492–4499, Jul. 2017, doi: 10.1109/JSEN.2017.2711432.

[28] T. Zhao, P. Li, and J. Cao, "Soft sensor modeling of chemical process based on self-organizing recurrent interval type-2 fuzzy neural network," *ISA Trans.*, vol. 84, pp. 237–246, Jan. 2019, doi: 10.1016/j.isatra.2018.10.014.

[29] J. Wang, K. Qiu, R. Wang, X. Zhou, and Y. Guo, "Development of Soft Sensor Based on Sequential Kernel Fuzzy Partitioning and Just-in-Time Relevance Vector Machine for Multiphase Batch Processes," *IEEE Trans. Instrum. Meas.*, vol. 70, pp. 1–10, 2021, doi: 10.1109/TIM.2021.3077970.

[30] M. Á. López Medina, M. Espinilla, C. Paggeti, and J. Medina Quero, "Activity Recognition for IoT Devices Using Fuzzy Spatio-Temporal Features as Environmental Sensor Fusion," *Sensors*, vol. 19, no. 16, p. 3512, Aug. 2019, doi: 10.3390/s19163512.

[31] J. Zhu, Y. Tang, X. Shao, and Y. Xie, "Multisensor Fusion Using Fuzzy Inference System for a Visual-IMU-Wheel Odometry," *IEEE Trans. Instrum. Meas.*, vol. 70, pp. 1–16, 2021, doi: 10.1109/TIM.2021.3051999.

[32] E. H. Mamdani and S. Assilian, "An experiment in linguistic synthesis with a fuzzy logic controller," *Int. J. Man. Mach. Stud.*, vol. 7, no. 1, pp. 1–13, Jan. 1975, doi: 10.1016/S0020-7373(75)80002-2.

[33] H. Li, Z. Wang, J. Y.-L. Forrest, and W. Jiang, "Low-Velocity Impact Localization on Composites Under Sensor Damage by Interpolation Reference Database and Fuzzy Evidence Theory," *IEEE Access*, vol. 6, pp. 31157–31168, 2018, doi: 10.1109/ACCESS.2018.2844802.

[34] M. Qian, Y. Yu, N. Ren, J. Wang, and X. Jin, "Sliding sensor using fiber Bragg grating for mechanical fingers," *Opt. Express*, vol. 26, no. 1, p. 254, Jan. 2018, doi: 10.1364/OE.26.000254.

[35] Z. Fu, Y. Zhao, H. Bao, and F. Zhao, "Dynamic Deformation Reconstruction of Variable Section WING with Fiber Bragg Grating Sensors," *Sensors*, vol. 19, no. 15, p. 3350, Jul. 2019, doi: 10.3390/s19153350.

[36] X. Hu, H. Si, H. Shen, and Z. Yu, "A fuzzy neural network model to determine axial strain measured by a long-period fiber grating sensor," *Meas. Control*, vol. 53, no. 3–4, pp. 704–710, Mar. 2020, doi: 10.1177/0020294019901307.

[37] A. Arslan and M. Kaya, "Determination of fuzzy logic membership functions using genetic algorithms," *Fuzzy Sets Syst.*, vol. 118, no. 2, pp. 297–306, Mar. 2001, doi: 10.1016/S0165-0114(99)00065-2.